A new method for information retrieval in two-dimensional grating-based X-ray phase contrast imaging*

Wang Zhi-Li(王志立)[a], Gao Kun(高 昆)[a], Chen Jian(陈 健)[a], Ge Xin(葛 昕)[a], Zhu Pei-Ping(朱佩平)[b], Tian Yang-Chao(田扬超)[a], and Wu Zi-Yu(吴自玉)[a)b)†]

[a] *National Synchrotron Radiation Laboratory, University of Science and Technology of China, Hefei* 230029, *China*
[b] *Institute of High Energy Physics, Chinese Academy of Sciences, Beijing* 100049, *China*

(Received 30 March 2012; revised manuscript received 1 June 2012)

Grating-based X-ray phase contrast imaging has been demonstrated to be an extremely powerful phase-sensitive imaging technique. By using two-dimensional (2D) gratings, the observable contrast is extended to two refraction directions. Recently, we have developed a novel reverse-projection (RP) method, which is capable of retrieving the object information efficiently with one-dimensional (1D) grating-based phase contrast imaging. In this contribution, we present its extension to the 2D grating-based X-ray phase contrast imaging, named the two-dimensional reverse-projection (2D-RP) method, for information retrieval. The method takes into account the nonlinear contributions of two refraction directions and allows the retrieval of the absorption, the horizontal and the vertical refraction images. The obtained information can be used for the reconstruction of the three-dimensional phase gradient field, and for an improved phase map retrieval and reconstruction. Numerical experiments are carried out, and the results confirm the validity of the 2D-RP method.

Keywords: X-ray imaging, phase contrast, information retrieval, shifting curve

PACS: 87.59.–e, 87.64.mh, 42.30.Rx **DOI:** 10.1088/1674-1056/21/11/118703

1. Introduction

X-ray imaging has been widely used for medical applications and non-destructive imaging since the discovery of X-rays in 1895. In conventional imaging, the contrast is generated through the differences in the absorption properties of the object. For weakly absorbing tissues, the use of conventional X-ray imaging is limited due to their weak absorptions and low image contrasts. To overcome this limitation, the X-ray phase contrast imaging has been developed and has attracted increasing attention since the 1990s.[1−11] With negligible anisotropy in the medium, the refractive index characterizing the optical properties of a tissue can be expressed as $n = 1 - \delta + \mathrm{i}\beta$, where δ is the decrement of the real part of the refractive index responsible for the phase shift, whereas the imaginary part β describes the absorption properties of the material. At diagnostically relevant photon energies and for soft tissues, the phase shift plays a more prominent role than the absorption, since δ is typically three orders of magnitude larger than β.[12] Therefore, phase contrast techniques are expected to yield improved contrasts and sensitivities when compared with the conventional absorption contrast imaging.

Recently, it has been demonstrated that grating-based X-ray phase contrast imaging is one of the most promising methods due to the advantages of high phase sensitivity, a large field of view,[13] and efficient utilization of conventional X-ray sources.[10,11] Momose *et al.*[7,8] and Pfeiffer *et al.*[9−11] have studied the phase contrast imaging using one-dimensional (1D) linear gratings. However, the 1D grating interferometer only gives contrasts for wavefront deviations or scatterings in the direction perpendicular to the grating lines, and it lacks sensitivity to object structures

*Project supported by the Knowledge Innovation Program of the Chinese Academy of Sciences (Grant No. KJCX2-YW-N42), the Key Project of the National Natural Science Foundation of China (Grant No. 10734070), the National Natural Science Foundation of China (Grant No. 11205157), the National Basic Research Program of China (Grant Nos. 2009CB930804 and 2012CB825800), the Fundamental Research Funds for the Central Universities, China (Grant No. WK2310000021), and the China Postdoctoral Science Foundation (Grant No. 2011M501064).

†Corresponding author. E-mail: wuzy@ustc.edu.cn

© 2012 Chinese Physical Society and IOP Publishing Ltd

oriented perpendicular to the lines. Additionally, the recovery of the phase map dose not require the exact knowledge of the boundary values, but induces substantial artifacts due to the lack of information on the blind direction.[14,15] In order to overcome these disadvantages, grating-based phase contrast imaging systems using two-dimensional (2D) structures have been developed. Wen *et al.*[16] and Zanette *et al.*[15] used a combination of closely stacked double linear gratings to form a 2D grating. Itoh *et al.* fabricated genuine 2D gratings and installed them in a 2D grating interferometer.[17,18]

In this contribution, we propose a novel method, named the 2D reverse-projection (RP) method, for information retrieval in 2D grating-based X-ray phase contrast imaging. As shown below, the two orthogonal refraction directions contribute in a nonlinear way to the recorded intensity. Thus, the 1D-RP method[19] cannot be directly applied to the 2D case for information retrieval. Therefore, we develop the 2D-RP method that takes into account the nonlinear contribution and allows the retrieval the absorption, horizontal and vertical refraction images.

2. Theory of the two-dimensional reverse-projection method

As schematically shown in Fig. 1, the setup of the 2D grating-based X-ray phase contrast imaging consists of a phase grating G1, an absorption analyzer grating G2, and an image detector. G1 has a checkerboard-type (CB-type) pattern and a thickness introducing π phase modulation at the incident X-ray energy. Detailed studies have shown that a CB-type π-shifting phase grating produces an interference distribution of square intensity spots.[20] The mesh-type (M-type) interference pattern with half the period of G1 is observed at the fractional Talbot distances $D_n = np_1^2/(8\lambda)$, where $n = 1, 3, 5, \ldots$, p_1 is the period of G1, and λ is the wavelength of the X-ray. The analyzer grating G2 located at the fractional Talbot distance has the same pattern as the self-image impinging on it. When a sample is placed in the beam, the interference pattern is distorted due to the refraction in the sample along two transverse directions. This distortion is analyzed by the G2 grating and is converted into intensity variations recorded by the image detector.

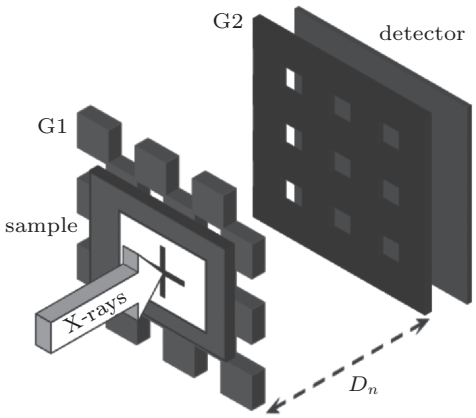


Fig. 1. Schematic diagram of the setup for 2D grating-based X-ray phase contrast imaging. With a sample placed in the X-ray beam, the interference pattern of the phase grating G1 is distorted by the sample refraction. The analyzer grating G2 converts this distortion into intensity variations measured by the detector.

The gratings used in the 2D grating-based phase contrast imaging can be either genuine 2D structures[17,18] or combinations of two 1D linear gratings.[15,16] As demonstrated in Fig. 2(a), the CB-type π-shifting phase grating G1 is equivalent to a superposition of two perpendicular 1D π-shifting phase gratings. Therefore, the amplitude transmission function of G1 can be expressed as the product of that of the two 1D π-shifting gratings

$$T(x,y) = T_1(x) \times T_1(y), \tag{1}$$

where $T_1(x)$ denotes the amplitude transmission function of a 1D π-shifting phase grating. Using the Fresnel diffraction formula, we can obtain the intensity of the self-image at position $(x_\mathrm{s}, y_\mathrm{s})$ in the self-image plane

$$\begin{aligned} I_\mathrm{s}(x_\mathrm{s}, y_\mathrm{s}) &= \left| A_0 \iint T(x,y) \exp\left[\frac{\mathrm{i}\pi (x_\mathrm{s}-x)^2}{\lambda D_n}\right] \right. \\ &\quad \left. \times \exp\left[\frac{\mathrm{i}\pi (y_\mathrm{s}-y)^2}{\lambda D_n}\right] \mathrm{d}x\mathrm{d}y \right|^2 \\ &= I_0 \left| \left\{ \int T_1(x) \exp\left[\frac{\mathrm{i}\pi (x_\mathrm{s}-x)^2}{\lambda D_n}\right] \mathrm{d}x \right\} \right|^2 \\ &\quad \times \left| \left\{ \int T_1(y) \exp\left[\frac{\mathrm{i}\pi (y_\mathrm{s}-y)^2}{\lambda D_n}\right] \mathrm{d}y \right\} \right|^2, \end{aligned} \tag{2}$$

with $I_0 = A_0^* A_0$ being the intensity incident on G1. As shown in Eq. (2), the self-image of G1 is the product of that of two orthogonal 1D π-shifting phase gratings, i.e, an M-type pattern.

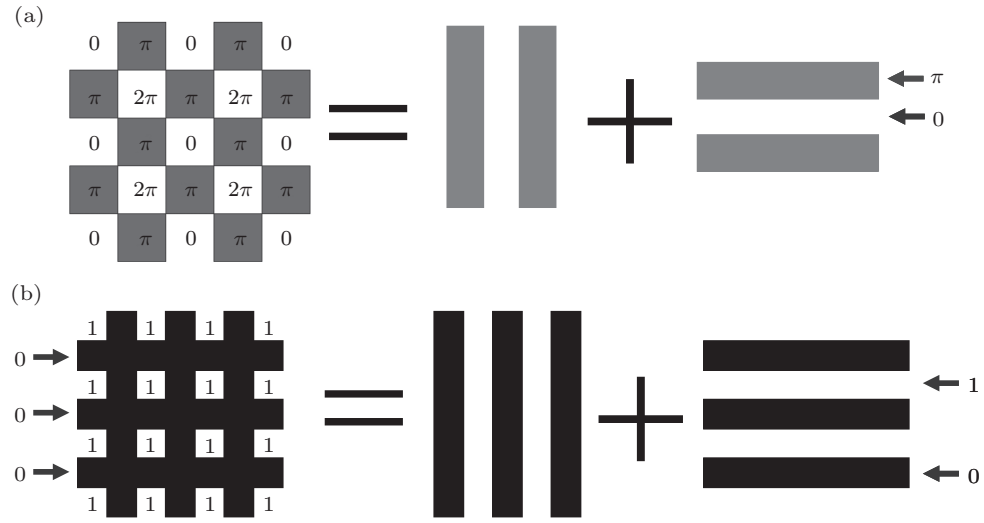


Fig. 2. (a) A 2D CB-type π-shifting grating is equivalent to the superposition of two crossed 1D π-shifting phase gratings. (b) The superposition of two perpendicular 1D absorption gratings results in a 2D M-type absorption grating.

For each detector pixel, the recorded intensity is the 2D convolution of the self-image pattern with the transmission function of G2

$$I(x,y) = I_{\mathrm{s}}(x_{\mathrm{s}}, y_{\mathrm{s}}) \otimes t(x,y), \tag{3}$$

where $\otimes$ denotes the 2D convolution operation. Similarly, a 2D M-type absorption grating can be obtained by a combination of two crossed linear absorption gratings, as shown in Fig. 2(b). The transmission function $t(x,y)$ can therefore be expressed as the product of that of two 1D absorption gratings

$$t(x,y) = t_1(x) \times t_1(y). \tag{4}$$

Substituting Eqs. (2) and (4) into Eq. (3), we can obtain the expression of the intensity distribution for each detector pixel

$$I(x,y) = I_0 \left[I_{\mathrm{s}}(x_{\mathrm{s}}) \otimes t_1(x) \right] \times \left[I_{\mathrm{s}}(y_{\mathrm{s}}) \otimes t_1(y) \right], \tag{5}$$

where $I_{\mathrm{s}}(x_{\mathrm{s}})$ represents the self-image of the 1D π-shifting phase grating

$$I_{\mathrm{s}}(x_{\mathrm{s}}) = \left| \left\{ \int T_1(x) \exp\left[\frac{\mathrm{i}\pi (x_{\mathrm{s}} - x)^2}{\lambda D_n} \right] \mathrm{d}x \right\} \right|^2. \tag{6}$$

By introducing the concept of the shifting curve (SC),[19] the recorded intensity can be equivalently written as

$$I(x_{\mathrm{g}}, y_{\mathrm{g}}) = I_0 S_x(x_{\mathrm{g}}) S_y(y_{\mathrm{g}}), \tag{7}$$

with x_{g} and y_{g} denoting the grating positions along the two transverse directions x and y, respectively. Equation (7) indicates that the detector signal in a single pixel is a function of grating positions x_{g} and y_{g}, as shown in Fig. 3(a). With a sample placed immediately in front of G1, the incident X-rays are not only attenuated but also refracted. The angular deviations from the beam direction due to the refraction in the sample are related to the phase gradient of the transmitted wave by[21]

$$\alpha_x = -\frac{\lambda}{2\pi} \frac{\partial \Phi(x,y)}{\partial x}, \quad \alpha_y = -\frac{\lambda}{2\pi} \frac{\partial \Phi(x,y)}{\partial y}, \tag{8}$$

where $\Phi(x,y)$ denotes the phase shift of the sample.

Within the approximation of geometrical optics, the intensity recorded by the detector can be expressed as (the corresponding equation in the case of 1D imaging can be found in Ref. [19])

$$\begin{aligned} I(x,y) = {} & I_{\mathrm{abs}}(x,y) S_x(x_{\mathrm{g}} + D_n \alpha_x) \\ & \times S_y(y_{\mathrm{g}} + D_n \alpha_y), \end{aligned} \tag{9}$$

where $I_{\mathrm{abs}}(x,y) = I_0 \exp\left(\int -\mu \mathrm{d}z\right)$ represents the absorption in the sample, $S_x(S_y)$ denotes the shifting curve in the x (y) direction, and x_{g} (y_{g}) defines the working point on the corresponding SC. In biomedical applications, the angular deviation is typically in the order of microradians, and the induced transverse shift is much smaller than $p_2/4$, i.e., $\alpha_x \ll p_2/4D_n$, $\alpha_y \ll p_2/4D_n$. This is supported by experimental evidence. Hasnah *et al.* found experimentally that the angular deviation caused by a 1 cm thick slice of breast tissue was in the order of 0.001 μrad to 0.01 μrad.[22] If the analyzer grating G2 is set at the half-slope position of the SC, as indicated in Fig. 3(b), the SCs in

Eq. (9) can be linearly approximated as

$$S_x\left(x_\mathrm{g}+D_n\alpha_x\right) \approx S_x\left(x_\mathrm{g}\right)+\frac{\partial S_x}{\partial x_\mathrm{g}}D_n\alpha_x,$$
$$S_y\left(y_\mathrm{g}+D_n\alpha_y\right) \approx S_y\left(y_\mathrm{g}\right)+\frac{\partial S_y}{\partial y_\mathrm{g}}D_n\alpha_y. \quad (10)$$

And we can have

$$I\left(x,y\right) = I_\mathrm{abs}\left(x,y\right)\left[S_x\left(x_\mathrm{g}\right)S_y\left(y_\mathrm{g}\right)+S_y\left(y_\mathrm{g}\right)C_x\alpha_x + S_x\left(x_\mathrm{g}\right)C_y\alpha_y+C_xC_y\alpha_x\alpha_y\right], \quad (11)$$

with $C_x = \left(\partial S_x/\partial x_\mathrm{g}\right)D_n$ and $C_y = \left(\partial S_y/\partial y_\mathrm{g}\right)D_n$. Note that the last term in Eq. (11) is not negligible and constitutes a nonlinear contribution of the perpendicular refraction directions to the detected intensity.

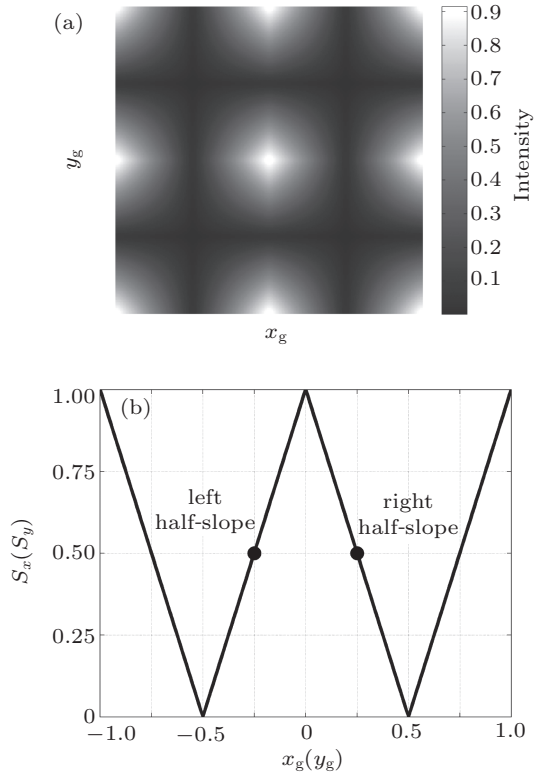


Fig. 3. (a) The recorded intensity in a single detector pixel as a function of the grating positions x_g and y_g. (b) Horizontal (vertical) shifting curve S_x (S_y) with respect to x_g (y_g) in units of p_2 assuming a fully coherent flat beam and perfect gratings.

In the proposed 2D-RP method, the analyzer grating G2 is fixed at the right half-slope position, i.e., $y_\mathrm{g} = p_2/4$, and is not further moved. Then four images are acquired: two (I_1 and I_3) on the left ($x_\mathrm{g}^\mathrm{l} = -p_2/4$) and the right ($x_\mathrm{g}^\mathrm{r} = p_2/4$) half-slope positions of the horizontal SC respectively. After the sample is rotated by 180° around the x axis, another two images (I_2 and I_4) are obtained again on the left and the right half-slope positions. According to Eq. (11), the corresponding image intensities are

$$I_1 = I_\mathrm{abs}[S_x\left(x_\mathrm{g}^\mathrm{l}\right)S_y\left(y_\mathrm{g}\right)+S_y\left(y_\mathrm{g}\right)C_{x\mathrm{l}}\alpha_x + S_x\left(x_\mathrm{g}^\mathrm{l}\right)C_y\alpha_y+C_{x\mathrm{l}}C_y\alpha_x\alpha_y], \quad (12)$$
$$I_2 = I_\mathrm{abs}[S_x\left(x_\mathrm{g}^\mathrm{l}\right)S_y\left(y_\mathrm{g}\right)+S_y\left(y_\mathrm{g}\right)C_{x\mathrm{l}}\alpha_x - S_x\left(x_\mathrm{g}^\mathrm{l}\right)C_y\alpha_y-C_{x\mathrm{l}}C_y\alpha_x\alpha_y], \quad (13)$$
$$I_3 = I_\mathrm{abs}[S_x\left(x_\mathrm{g}^\mathrm{r}\right)S_y\left(y_\mathrm{g}\right)+S_y\left(y_\mathrm{g}\right)C_{x\mathrm{r}}\alpha_x + S_x\left(x_\mathrm{g}^\mathrm{r}\right)C_y\alpha_y+C_{x\mathrm{r}}C_y\alpha_x\alpha_y], \quad (14)$$
$$I_4 = I_\mathrm{abs}[S_x\left(x_\mathrm{g}^\mathrm{r}\right)S_y\left(y_\mathrm{g}\right)+S_y\left(y_\mathrm{g}\right)C_{x\mathrm{r}}\alpha_x - S_x\left(x_\mathrm{g}^\mathrm{r}\right)C_y\alpha_y-C_{x\mathrm{r}}C_y\alpha_x\alpha_y], \quad (15)$$

where $S_x\left(x_\mathrm{g}^\mathrm{l}\right)$ and $C_{x\mathrm{l}}$ ($S_x\left(x_\mathrm{g}^\mathrm{r}\right)$ and $C_{x\mathrm{r}}$) are the parameters for S_x at the left (right) half-slope position, and $C_y = [\partial S_y\left(p_2/4\right)/\partial y_\mathrm{g}]D_n$. In the above formulas, we have utilized the fact that the sample rotation of 180° is equivalent to the inversion of the corresponding refraction direction.[19] The 2D-RP method is introduced by solving the set of four nonlinear equations (Eqs. (12)–(15)] for the three unknowns I_abs, α_x, and α_y. As presented in Appendix A, the solution for the apparent absorption image I_abs is

$$I_\mathrm{abs} = \frac{C_{x\mathrm{r}}\left(I_1+I_2\right)-C_{x\mathrm{l}}\left(I_3+I_4\right)}{2S_y\left(y_\mathrm{g}\right)\left[S_x\left(x_\mathrm{g}^\mathrm{l}\right)C_{x\mathrm{r}}-S_x\left(x_\mathrm{g}^\mathrm{r}\right)C_{x\mathrm{l}}\right]}, \quad (16)$$

while the horizontal refraction image α_x is given by

$$\alpha_x = \frac{S_x\left(x_\mathrm{g}^\mathrm{r}\right)\left(I_1+I_2\right)-S_x\left(x_\mathrm{g}^\mathrm{l}\right)\left(I_3+I_4\right)}{C_{x\mathrm{l}}\left(I_3+I_4\right)-C_{x\mathrm{r}}\left(I_1+I_2\right)}, \quad (17)$$

and the vertical refraction image α_y is

$$\alpha_y = \frac{I_1-I_2}{I_1+I_2}\frac{S_y\left(y_\mathrm{g}\right)}{C_y}. \quad (18)$$

Alternatively, the 2D-RP method can also be performed by fixing the grating G2 at either slope position of the horizontal SC and rotating the sample by 180° around the y axis. The corresponding solutions for the three images are presented in Appendix B.

3. Results and discussion

Numerical experiments are carried out to demonstrate the feasibility and effectiveness of the proposed 2D-RP method. The setup assumed for the simulations resembles the experimental setup presented by Zanette *et al.*[15] The incident X-ray energy is 30 keV. The 2D grating interferometer consists of a CB-type π-shifting phase grating with a period of $p_1 = 4$ μm, and an M-type absorption grating with a period of $p_2 = 2$ μm. The distance between the two gratings is $D_3 = 14.5$ cm (the 3rd fractional Talbot distance). In

the simulations, we assume that the sample is placed in the phase grating plane, and the detector is at the analyzer grating plane; whilst in experiments, the sample is placed immediately upstream of G1, and the detector is placed as close as possible to G2.

The investigated object consists of two crossed plastic cylinders of 8 mm diameter. According to the 2D-RP method, four images are recorded at the predefined grating positions. The image intensities are calculated using Eq. (9), and one of them is shown in Fig. 4(a). We have applied the 2D-RP method to the simulated data, and retrieved the absorption and the refraction images of the object. The results are shown in Figs. 4(b)–4(d) respectively. To present the quality of the retrieved sample images, quantitative comparisons of the line profiles between the retrieved results and the theoretical predications are performed, and the results are shown in Figs. 5(a) and 5(b). The locations of the extracted line profiles are indicated by AA' in Fig. 4(b). As can be seen, there is an excellent agreement between the results of the 2D-RP method and the theoretical predications, thus confirming the validity of the 2D-RP method. On the one hand, we note that large values of refraction are underestimated by the 2D-RP method, as shown in Fig. 5(b). This is attributed to a violation of the validity of the linear approximation of the SC (Eq. (10)). The comparison of the dynamic range ($\sim$ 3.5 μrad) and the largest refraction angle value (4.3 μrad) support this explanation. In addition, the 2D-RP method makes use of only four images for information retrieval, which is advantageous in terms of the total exposure time and potential radiation dose.

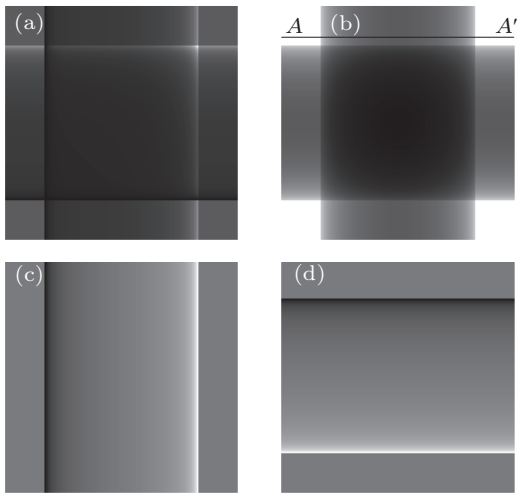


Fig. 4. (a) One of recorded images in the 2D-RP method. (b) Retrieved absorption image. (c) Retrieved horizontal refraction image. (d) Retrieved vertical refraction image.

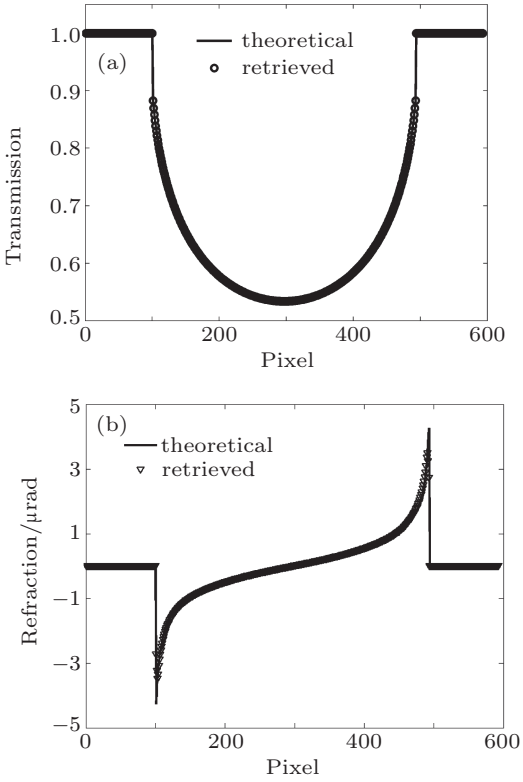


Fig. 5. Retrieved line profiles along AA' compared with theoretical predications for (a) the absorption and (b) the refraction images respectively.

Compared to the 2D phase stepping technique,[15] the introduced 2D-RP method only moves one of the gratings in one dimension, thus simplifying the experimental procedure and increasing the data acquisition. With respect to single-shot Fourier transform approaches,[17,18] the presented 2D-RP method retains the full spatial resolution of the detector in the retrieved images. Compared with the approach presented by Rutishauser *et al.*,[23] the use of 2D gratings is rewarded by a higher sensitivity.

In the presented simulations, we have assumed a fully coherent flat beam and perfect gratings. Actually, the performance of the 2D grating interferometer is affected by factors such as polychromaticity and imperfect spatial coherence of incident X-rays. Considerations concerning performance aspects of 1D grating interferometers can also be applied to the 2D grating interferometer.[24−27] In further work, detailed analysis will be presented on the influence of these factors on the performance of the 2D-RP method.

4. Conclusion

In conclusion, we have introduced the two-dimensional reverse-projection method for information retrieval in 2D grating-based X-ray phase contrast imaging, and demonstrated its applicability to quantitative retrieval of the absorption, horizontal and vertical refraction images. The results of numerical experiments verify the validity of the 2D-RP method. It takes into account the nonlinear contribution of two perpendicular refraction directions to the recorded intensity. The 2D-RP method requires no more than four experimental images per projection, which is advantageous concerning total exposure time and potential radiation damage.

For further analysis, the obtained phase gradient information can be used for the three-dimensional reconstruction of the phase gradient field[28,29] and for an improved phase map retrieval and reconstruction.[14,15] The presented 2D-RP method is also applicable to the 2D Talbot–Lau interferometer.[18] We can expect a wide application of the 2D-RP method in biomedical imaging, material sciences, and so on.

Appendix A: Derivation of Eqs. (16)–(18)

From Eqs. (12)–(15), we can obtain

$$I_1 + I_2 = 2I_{\rm abs}[S_x\left(x_{\rm g}^{\rm l}\right) S_y\left(y_{\rm g}\right) + S_y\left(y_{\rm g}\right) C_{x{\rm l}}\alpha_x], \quad \text{(A1)}$$

$$I_3 + I_4 = 2I_{\rm abs}[S_x\left(x_{\rm g}^{\rm r}\right) S_y\left(y_{\rm g}\right) + S_y\left(y_{\rm g}\right) C_{x{\rm r}}\alpha_x]. \quad \text{(A2)}$$

From a combination of Eqs. (A1) and (A2), we can have

$$\begin{aligned} &C_{x{\rm r}}\left(I_1 + I_2\right) - C_{x{\rm l}}\left(I_3 + I_4\right) \\ &= 2I_{\rm abs}[S_x\left(x_{\rm g}^{\rm l}\right) S_y\left(y_{\rm g}\right) C_{x{\rm r}} \\ &\quad - S_x\left(x_{\rm g}^{\rm r}\right) S_y\left(y_{\rm g}\right) C_{x{\rm l}}]. \end{aligned} \quad \text{(A3)}$$

And the solution for the apparent absorption image $I_{\rm abs}$ is

$$I_{\rm abs} = \frac{C_{x{\rm r}}\left(I_1 + I_2\right) - C_{x{\rm l}}\left(I_3 + I_4\right)}{2S_y\left(y_{\rm g}\right)\left[S_x\left(x_{\rm g}^{\rm l}\right) C_{x{\rm r}} - S_x\left(x_{\rm g}^{\rm r}\right) C_{x{\rm l}}\right]}. \quad \text{(A4)}$$

Substituting Eq. (A4) into Eq. (A1), we can obtain the horizontal refraction image

$$\alpha_x = \frac{S_x\left(x_{\rm g}^{\rm r}\right)\left(I_1 + I_2\right) - S_x\left(x_{\rm g}^{\rm l}\right)\left(I_3 + I_4\right)}{C_{x{\rm l}}\left(I_3 + I_4\right) - C_{x{\rm r}}\left(I_1 + I_2\right)}. \quad \text{(A5)}$$

The vertical refraction image can be obtained by the substitution of Eqs. (A4) and (A5) into Eq. (12)

$$\alpha_y = \frac{I_1 - I_2}{I_1 + I_2}\frac{S_y\left(y_{\rm g}\right)}{C_y}. \quad \text{(A6)}$$

Appendix B: Alternative approach of the 2D-RP method

Alternatively, the 2D-RP method can be performed by fixing G2 at the slope position of the horizontal SC, i.e., $x_{\rm g} = -p_2/4$ or $x_{\rm g} = p_2/4$. Two images (I_1 and I_3) are recorded on the left ($y_{\rm g}^{\rm l} = -p_2/4$) and the right ($y_{\rm g}^{\rm r} = p_2/4$) half-slope positions of the vertical SC respectively. Then we rotate the sample by 180° around the y axis, and record another two images (I_2 and I_4) on the left and the right half-slope positions respectively. The recorded image intensities are given by

$$\begin{aligned} I_1 = I_{\rm abs}[&S_x\left(x_{\rm g}\right) S_y\left(y_{\rm g}^{\rm l}\right) + S_y\left(y_{\rm g}^{\rm l}\right) C_x\alpha_x \\ &+ S_x\left(x_{\rm g}\right) C_{y{\rm l}}\alpha_y + C_x C_{y{\rm l}}\alpha_x\alpha_y], \end{aligned} \quad \text{(B1)}$$

$$\begin{aligned} I_2 = I_{\rm abs}[&S_x\left(x_{\rm g}\right) S_y\left(y_{\rm g}^{\rm l}\right) - S_y\left(y_{\rm g}^{\rm l}\right) C_x\alpha_x \\ &+ S_x\left(x_{\rm g}\right) C_{y{\rm l}}\alpha_y - C_x C_{y{\rm l}}\alpha_x\alpha_y], \end{aligned} \quad \text{(B2)}$$

$$\begin{aligned} I_3 = I_{\rm abs}[&S_x\left(x_{\rm g}\right) S_y\left(y_{\rm g}^{\rm r}\right) + S_y\left(y_{\rm g}^{\rm r}\right) C_x\alpha_x \\ &+ S_x\left(x_{\rm g}\right) C_{y{\rm r}}\alpha_y + C_x C_{y{\rm r}}\alpha_x\alpha_y], \end{aligned} \quad \text{(B3)}$$

$$\begin{aligned} I_4 = I_{\rm abs}[&S_x\left(x_{\rm g}\right) S_y\left(y_{\rm g}^{\rm r}\right) - S_y\left(y_{\rm g}^{\rm r}\right) C_x\alpha_x \\ &+ S_x\left(x_{\rm g}\right) C_{y{\rm r}}\alpha_y - C_x C_{y{\rm r}}\alpha_x\alpha_y], \end{aligned} \quad \text{(B4)}$$

with $C_x = [\partial S_x\left(p_2/4\right)/\partial x_{\rm g}]D_n$. Following the procedure presented in Appendix A, we can obtain the solutions for the three unknowns $I_{\rm abs}$, α_y and α_x

$$I_{\rm abs} = \frac{C_{y{\rm r}}\left(I_1 + I_2\right) - C_{y{\rm l}}\left(I_3 + I_4\right)}{2S_x\left(x_{\rm g}\right)\left[S_y\left(y_{\rm g}^{\rm l}\right) C_{y{\rm r}} - S_y\left(y_{\rm g}^{\rm r}\right) C_{y{\rm l}}\right]}, \quad \text{(B5)}$$

$$\alpha_y = \frac{S_y\left(y_{\rm g}^{\rm r}\right)\left(I_1 + I_2\right) - S_y\left(y_{\rm g}^{\rm l}\right)\left(I_3 + I_4\right)}{C_{y{\rm l}}\left(I_3 + I_4\right) - C_{y{\rm r}}\left(I_1 + I_2\right)}, \quad \text{(B6)}$$

$$\alpha_x = \frac{I_1 - I_2}{I_1 + I_2}\frac{S_x\left(x_{\rm g}\right)}{C_x}. \quad \text{(B7)}$$

References

[1] Bonse U and Hart M 1965 *Appl. Phys. Lett.* **6** 155
[2] Momose A, Takeda T, Itai Y and Hirano K 1996 *Nature Med.* **2** 473
[3] Nugent K, Gureyev T, Cookson D, Paganin D and Barnea Z 1996 *Phys. Rev. Lett.* **77** 2961
[4] Wilkins S, Gureyev T, Gao D, Pogany A and Stevenson A 1996 *Nature* **384** 335
[5] Davis T, Gao D, Gureyev T, Stevenson A and Wilkins S 1995 *Nature* **373** 595
[6] Chapman D, Thomlinson W, Johnston R, Washburn D, Pisano E, Gmur N, Zhong Z, Menk R, Arfelli F and Sayers D 1997 *Phys. Med. Biol.* **42** 2015

[7] Momose A, Kawamoto S, Koyama I, Hamaishi Y, Takai K and Suzuki Y 2003 *Jpn. J. Appl. Phys.* **42** L866

[8] Momose A, Yashiro W, Takeda Y, Suzuki Y and Hattori T 2006 *Jpn. J. Appl. Phys.* **45** 5254

[9] Weitkamp T, Daiz A, David C, Pfeiffer F, Stampanoni M, Cloetens P and Ziegler E 2005 *Opt. Express* **13** 6296

[10] Pfeiffer F, Weitkamp T, Bunk O and David C 2006 *Nature Phys.* **2** 258

[11] Pfeiffer F, Bech M, Bunk O, Kraft P, Eikenberry E, Bronnimann Ch, Grunzweig C and David C 2008 *Nature Mater.* **7** 134

[12] Momose A and Fukuda J 1995 *Med. Phys.* **22** 375

[13] Revol V, Kottler C, Kaufmann R, Jerjen I, Luthi T, Cardot F, Niedermann P, Straumann U, Sennhauser U and Urban C 2011 *Nucl. Instrum. Meth.* A **648** S302

[14] Kotter C, David C, Pfeiffer F and Bunk O 2007 *Opt. Express* **15** 1175

[15] Zanette I, Weitkamp T, Donath T, Rutishauser S and David C 2010 *Phys. Rev. Lett.* **105** 248102

[16] Wen H H, Bennet E E, Kopace R, Stein A F and Pai V 2010 *Opt. Lett.* **35** 1932

[17] Itoh H, Nagai K, Sato G, Yamaguchi K, Nakamura T, Kondoh T, Ouchi C, Teshima T, Setomoto Y and Den T 2011 *Opt. Express* **19** 3339

[18] Sato G, Kondoh T, Itoh H, Handa S, Yamaguchi K, Nakamura T, Nagai K, Ouchi C, Teshima T, Setomoto Y and Den T 2011 *Opt. Lett.* **36** 3551

[19] Zhu P P, Zhang K, Wang Z L, Liu Y J, Liu X S, Wu Z Y, McDonald S A, Marone F and Stampanoni M 2010 *Proc Natl. Acad. Sci. USA* **107** 13576

[20] Zanette I, David C, Rutishauser S and Weitkamp T 2010 *AIP Conf. Proc.* **1221** 73

[21] Born M and Wolf E 1999 *Principles of Optics* (7th edn.) (New York: Cambridge University Press) p. 562

[22] Hasnah M O, Oltulu O, Chapman D, Zhong Z, Pisano E, Johnston R E, Sayers D and Thomlinson W 2002 *Med. Phys.* **29** 2216

[23] Rutishauser S, Donath T, David C, Pferiffer F, Marone F, Modregger P and Stampanani M 2011 *Opt. Express* **19** 24890

[24] Wang Z L, Liu X S, Zhu P P, Huang W X, Yuan Q X, Li E R, Liu Y J, Zhang K, Hong Y L and Wu Z Y 2010 *Nucl. Instrum. Meth.* A **619** 319

[25] Ge X, Wang Z L, Gao K, Zhang K, Hong Y L, Wang D J, Zhu Z Z, Zhu P P and Wu Z Y 2011 *Anal. Bioanal. Chem.* **401** 865

[26] Wang Z L, Zhu P P, Huang W X, Yuan Q X, Liu X S, Zhang K, Hong Y L, Zhang H T, Ge X, Gao K and Wu Z Y 2010 *Anal. Bioanal. Chem.* **397** 2091

[27] Wang Z L, Zhu P P, Huang W X, Yuan Q X, Liu X S, Zhang K, Hong Y L, Zhang H T, Ge X, Gao K and Wu Z Y 2010 *Anal. Bioanal. Chem.* **397** 2137

[28] Zhu P P, Wang J Y, Yuan Q X, Huang W X, Shu H, Gao B, Hu T D and Wu Z Y 2005 *Appl. Phys. Lett.* **87** 264101

[29] Wang J Y, Zhu P P, Yuan Q X, Huang W X, Shu H, Chen B, Hu T D and Wu Z Y 2006 *Phys. Med. Biol.* **51** 3391